Structural Elucidation and Absolute Stereochemistry for Pharma Compounds using MicroED

Lygia Silva de Moraes[1‡], Jessica E. Burch[1,2,5‡], David A. Delgadillo[1], Isabel Hernandez Rodriguez[1], Huanghao Mai[1], Austin G. Smith[3†], Seb Caille[3], Shawn D. Walker[3†], Ryan P. Wurz[4], Victor J. Cee[4†], Jose A. Rodriguez[2], Dan Gostovic[5], Kyle Quasdorf[3*], Hosea M. Nelson[1,2*]

[1] Division of Chemistry and Chemical Engineering, California Institute of Technology, Pasadena, California 91125, United States.

[2] Department of Chemistry and Biochemistry, University of California, Los Angeles, Los Angeles, California 90095, United States.

[3] Drug Substance Technologies - Synthetics, Process Development [4] Medicinal Chemistry, Amgen Inc., One Amgen Center Drive, Thousand Oaks, California 91320, United States.

[5] MicroEDLab.com, 1623 Central Avenue Suite 18, Cheyenne, Wyoming 82001, United States.

*Correspondence to: quasdorf@amgen.com, hosea@caltech.edu

Supporting Information

Contents

1. Materials

Table S1. Fifteen pharmaceutical compounds analyzed in this study.

Compound	Name	Compound Source	References	Datasets collected
1	(2R,3S)-N-(4-(2,6-dimethoxyphenyl)-5-(5-methylpyridin-3-yl)-4H-1,2,4-triazol- 3-yl)-3-(5-methylpyrimidin-2-yl)butane-2-sulfonamide	Medicinal Chemistry	[1]	6
2	(2R,3S)-3-(5-methoxypyridin-2-yl)butane-2-sulfonamide	Medicinal Chemistry	[1,2]	3
3	(2S,3R)-N-(4-(2,6-dimethoxyphenyl)-5-(5-methylpyridin-3-yl)-4H-1,2,4-triazol-3-yl)-3-(5-methylpyrimidin-2-yl)butane-2-sulfonamide	Medicinal Chemistry	[1]	18
4	(2S,3R)-3-(5-methoxypyridin-2-yl)butane-2-sulfonamide	Medicinal Chemistry	[1,2]	23
5	(R)-6'-chloro-3',4,4',5-tetrahydro-2H,2'H-spiro[benzo[b][1,4]oxazepine-3,1'-naphthalene]-7-carboxylic acid ((1R,4S)-7,7-dimethyl-2-oxobicyclo[2.2.1]heptan-1- yl)methansulfonate	Process Chemistry	[3]	8
6	(2S,3R)-3-(5-methylpyrazin-2-yl)butane-2-sulfonamide	Medicinal Chemistry	[1,2,4–8]	9
7	(1S,3'R,6'R,7'S,8'E,11'S,12'R)-6-chloro-7'-hydroxy-11',12'-dimethyl-3,4-dihydro-2H,15'H-spiro[naphthalene-1,22'-[20]oxa[13]thia[1,14]diazatetracyclo [14.7.2.03,6.019,24]pentacosa[8,16,18,24]tetraen]-15'-one 13',13'-dioxide	Process Chemistry	[3]	10
8	(S)-6'-chloro-3',4,4',5-tetrahydro-2H,2'H-spiro[benzo[b][1,4]oxazepine-3,1'-naphthalene]-7-carboxylic acid ((1S,4R)-7,7-dimethyl-2-oxobicyclo[2.2.1]heptan-1- yl)methansulfonate	Process Chemistry	[3]	8
9	(S)-6'-chloro-5-(((1R,2R)-2-((S)-1-hydroxyallyl)cyclobutyl)methyl)-N-(((2R,3S)- 3-methylhex-5-en-2-yl)sulfonyl)-3',4,4',5-tetrahydro-2H,2'H-spiro[benzo[B][1,4] oxazepine-3,1'-naphthalene]-7-carboxamide	Process Chemistry	[3]	12
10	(R)-1-phenylethan-1-aminium (S)-6'-chloro-5-(((1R,2R)-2-((S)-1-hydroxyallyl)cyclobutyl)methyl)-3',4,4',5-tetrahydro-2H,2'H-spiro[benzo[b][1,4]oxazepine-3,1'- naphthalene]-7-carboxylate	Process Chemistry	[3]	2
11	(S)-1-(5-fluoropyrimidin-2-yl)piperidine-3-sulfonamide	Medicinal Chemistry	[4,6]	8
12	(2R,3S)-3-(5-methylpyrazin-2-yl)butane-2-sulfonamide	Medicinal Chemistry	[1,2,4–8]	3
13	(R)-1-(5-fluoropyrimidin-2-yl)piperidine-3-sulfonamide	Medicinal Chemistry	[4,6]	4
14	(2R,3S)-3-methylhex-5-ene-2-sulfonamide	Process Chemistry	[9]	5
15	methyl piperazine-1-carboxylate phosphate hydrate	Process Chemistry	[10]	15
	Figure 5a	Medicinal Chemistry	[11-13]	-
	Figure 5b	PROTACs	[14]	-

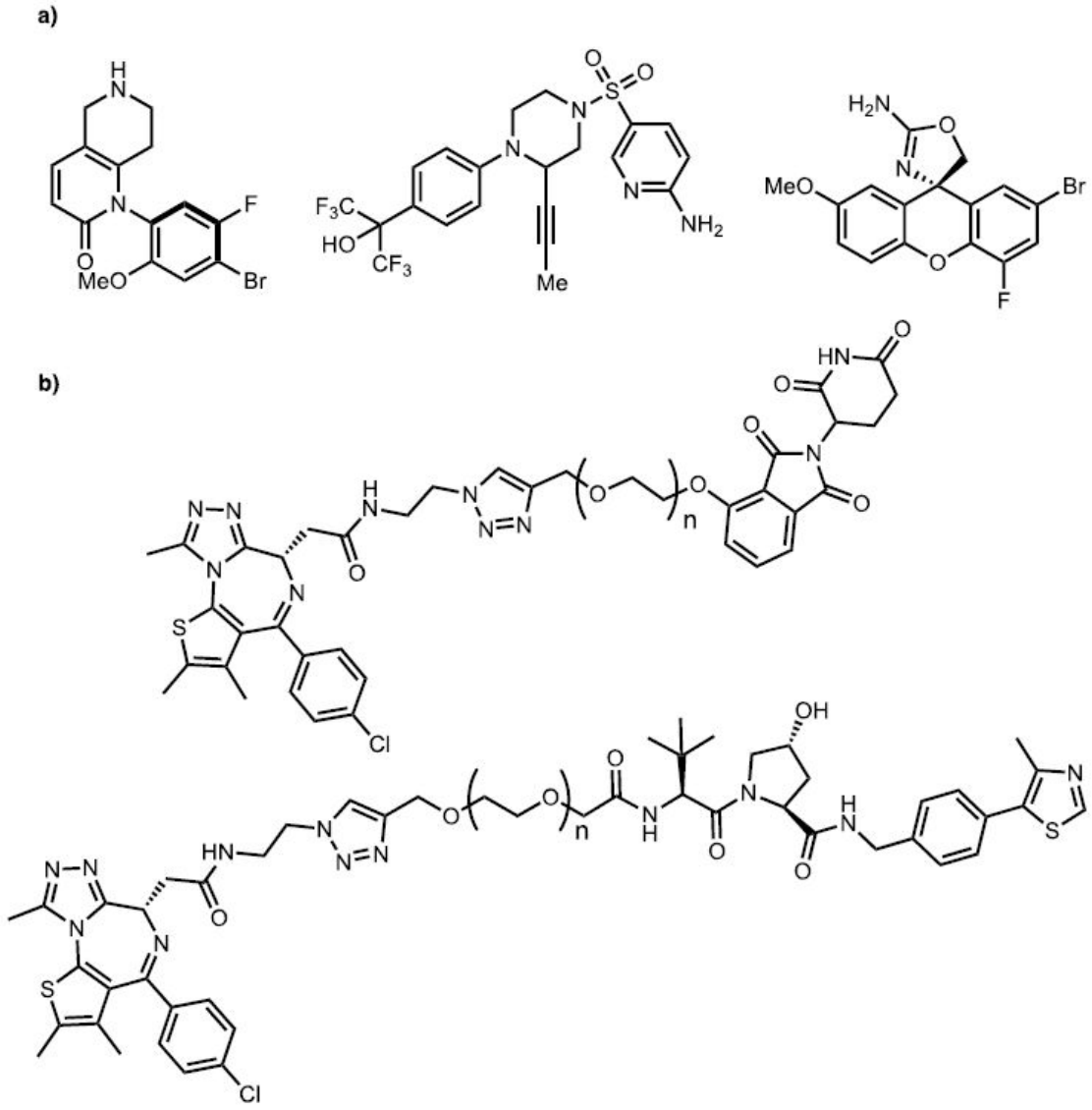

Figure S1. Molecular structure of remaining fifteen compounds not solved with microED, where (a) illustrates enantiomeric pairs (only one enantiomer drawn) and (b) illustrates PROTACs, n = 0–4.

2. Available instruments for microED

a. Thermo Fisher Scientific TEMs with microED package: https://www.thermofisher.com/br/en/home/electron-microscopy/products/transmission-electron-microscopes.html
b. Rigaku Synergy-ED: https://www.synergy-ed.com/
c. Eldico scientific ED-1: https://www.eldico-scientific.com/

3. General microcrystal electron diffraction experiment

All diffraction experiments were performed in a Thermo Fisher Scientific Talos F200C transmission electron microscope equipped with a Ceta-D detector operating at an accelerating voltage of 200 keV. To screen for crystallinity, particles were located on the grid in imaging mode at 2600x magnification. After identifying a particle of interest, a diffraction pattern was recorded by isolating a region of the

particle using a selected area aperture and entering parallel-illuminated diffraction mode utilizing the low dose software on the Thermo Fisher microscope user interface.

A single image of the diffraction pattern was taken on a Thermo Fisher Scientific Ceta-D camera. If user inspection of the diffraction pattern suggested that the particle was monocrystalline and provided <1.2 Å resolution diffraction, the eucentric height of the sample was adjusted in imaging mode to ensure the crystal would remain within the selected area aperture throughout a tilt series with a maximum tilt range of ± 65°. After making these adjustments and returning to diffraction mode, a continuously rotating electron diffraction movie was collected by rotating the stage at a rate of 0.3° s^{-1}. The Ceta-D CMOS 4k x 4k camera was operated using rolling shutter mode and continuously integrated at a rate of 3 seconds per frame with binning by 2 to produce 2k x 2k images. Diffraction movies were saved as SER files. Movies were saved with a standardized naming format and processed using the automated data workflow while additional movies were collected. These processed movies were manually re-indexed to different space groups and/or merged with other datasets as needed until preliminary solutions were obtained.

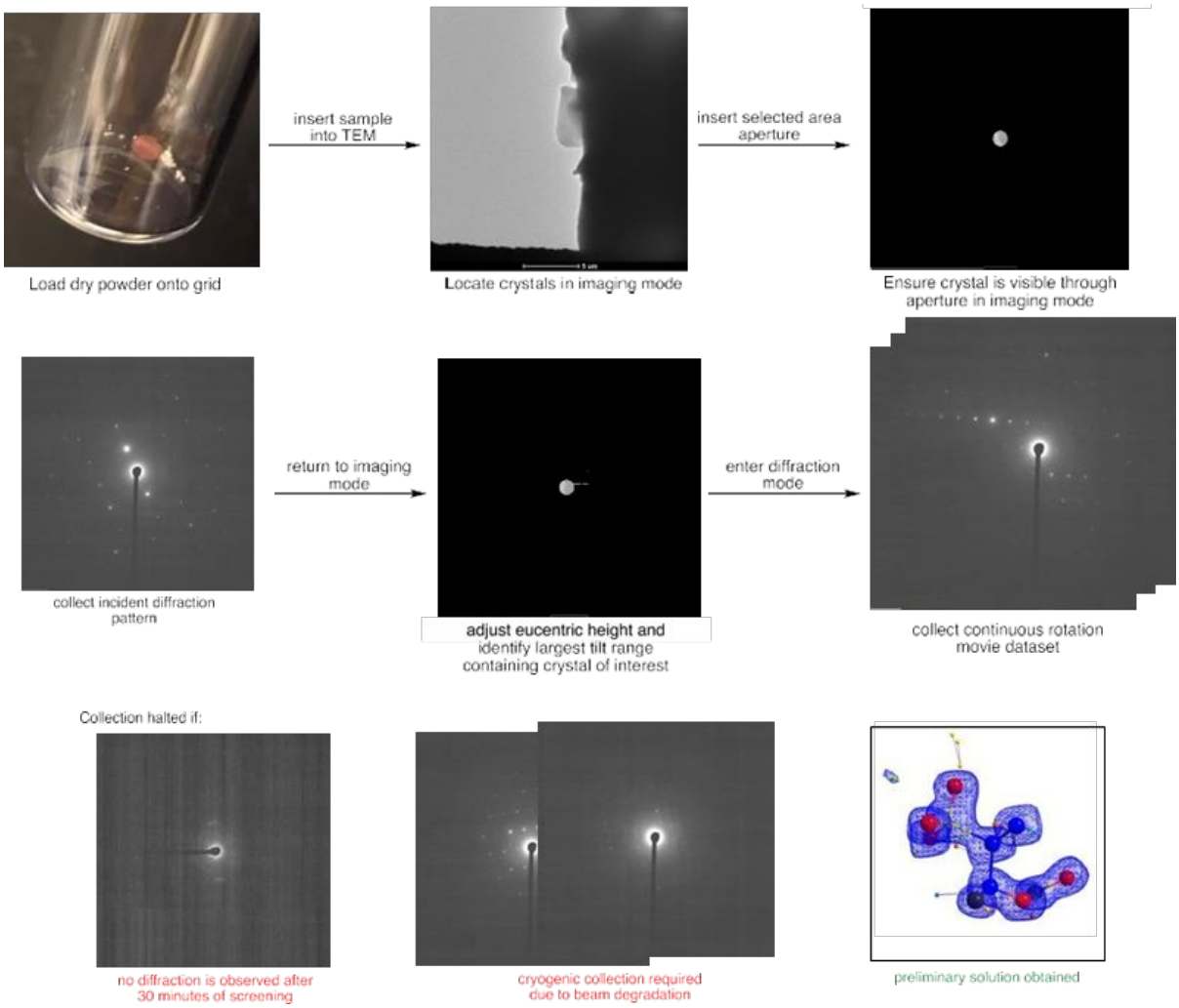

Figure S2. Representative data collection workflow.

4. Room temperature TEM screening procedure

Milligram to sub-milligram quantities of dry powder were placed into a dram vial as received and manually ground with a glass pipette. A pure carbon 200 mesh Cu grid or lacey carbon Cu grid was

placed inside of the vial and gently shaken together with the powder to “dry load” the grid (Figure S2). The grid was removed with Dumont straight self-closing tweezers and the tweezers were gently tapped against a lab bench while holding the grid to shake off excess powder. This sample was clipped into a single tilt holder and inserted into a well-aligned Thermo Fisher Scientific Talos F200C transmission electron microscopy for microED experiments using the experimental procedure described in the Supporting Information File, Section 2. Screening was halted if no diffraction was observed after 30 minutes, the sample visibly lost resolution over the course of a single movie, or a preliminary solution with >90% of expected atoms was obtained. Results for samples **1**-**6** are observed in Figure S3 and Table S2,

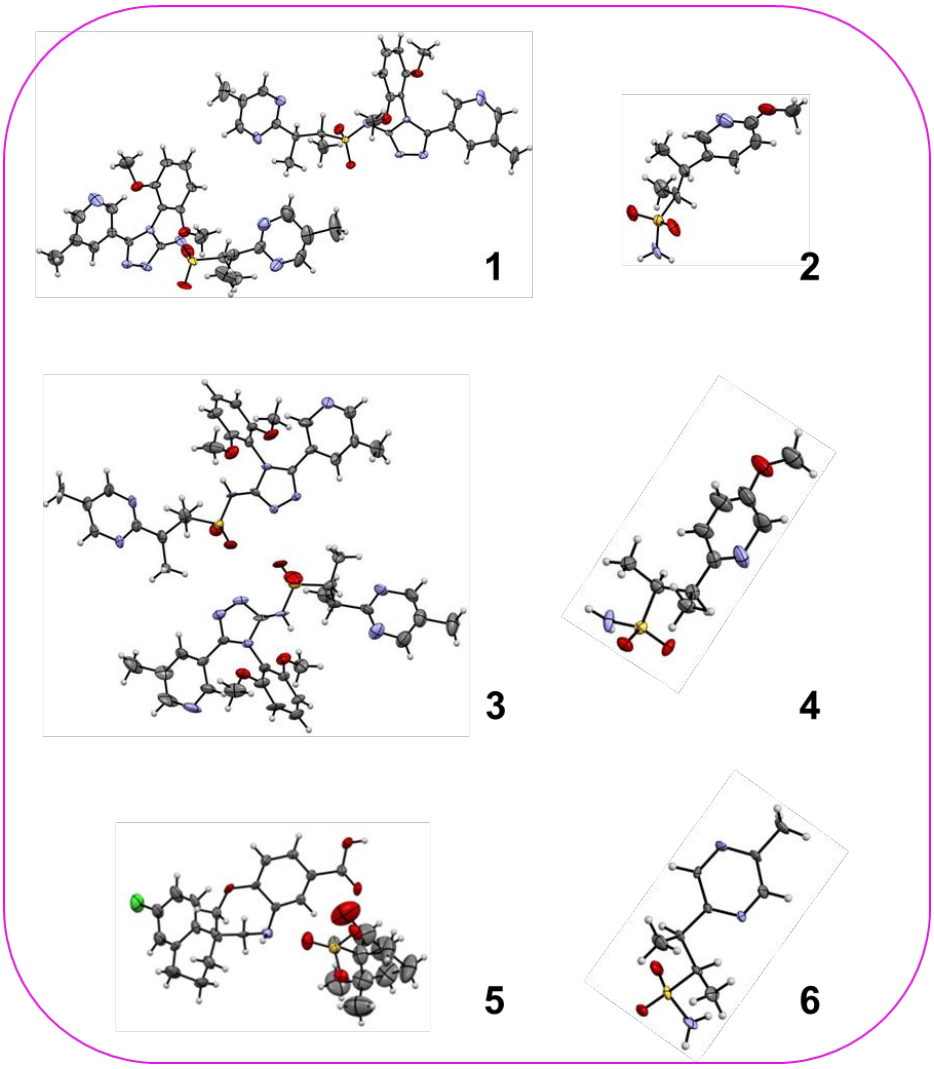

Figure S3. Contents of the asymmetric unit of compounds **1**-**6** obtained by room temperature screening. Ellipsoids probability: 50 %

Table S2. Selected crystallographic data for compounds **1**-**6** screened at room temperature.

Compound	**1**	**2**	**3**	**4**	**5**	**6**
Empirical formula	$C_{25}H_{29}N_7O_4S$	$C_{10}H_{16}N_2O_3S$	$C_{25}H_{29}N_7O_4S$	$C_{10}H_{16}N_2O_3S$	$C_{29}H_{34}NO_7SCl$	$C_9H_{15}N_3O_2S$
Formula weight	523.61	244.31	523.61	244.31	574.07	229.3
Data Collection						
Type of instrument	Talos F200C	Talos F200C	Talos F200C	Talos F200C	Talos F200C	Talos F200C
Wavelength (Å)	0.0251	0.0251	0.0251	0.0251	0.0251	0.0251
Data collection temperature (K)	294(2)	294(2)	294(2)	294(2)	294(2)	294(2)
Unit cell dimensions	*a* = 9.3100(10) Å, *b* = 20.490(2) Å, *c* = 12.650(4) Å, *β* = 108.42 °	*a* = 22.830(4) Å, *b* = 6.810(10) Å, *c* = 6.980(2) Å	*a* = 9.3100(10) Å, *b* = 20.450(2) Å, *c* = 12.680(4) Å, *β* = 108.40 °	*a* = 6.840(2) Å, *b* = 22.820(4) Å, *c* = 6.9800(10) Å	*a* = 10.5200(10) Å, *b* = 10.220(2) Å, *c* = 12.660(4) Å, *β* = 110.33 °	*a* = 7.4500(10) Å, *b* = 8.130(2) Å, *c* = 16.240(4) Å
Volume	2289.5(8)	1085.2(4)	2290.7(8)	1089.5(4)	1276.4(5)	983.6(4)
Z, Z'	2, 2	4, 1	2, 2	4, 1	2, 1	4, 1
Crystal system	Monoclinic	Orthorhombic	Monoclinic	Orthorhombic	Monoclinic	Orthorhombic
Space group	$P2_1$	$P2_12_12$	$P2_1$	$P2_12_12$	$P2_1$	$P2_12_12_1$
Density (calculated) (g/cm^3)	1.515	1.495	1.518	1.489	1.494	1.548
F(000)	100	103	100	103	99	46
Measured reflections	6341	3816	5615	1212	2438	1652
Reflections with I > 2s(I)	3849	870	3218	649	1379	975
Resolution (Å)	0.90	0.95	0.90	0.95	1.00	0.80
Completeness (%)	81.40	82.90	85.50	89.40	95.70	82.60
Index ranges	10 ≤ h ≤ -10, 23 ≤ k ≤ -24, 13 ≤ l ≤ -13	7 ≤ h ≤ -7, 25 ≤ k ≤ -25, 7 ≤ l ≤ -7	10 ≤ h ≤ -10, 21 ≤ k ≤ -21, 14 ≤ l ≤ -14	24 ≤ h ≤ -24, 7 ≤ k ≤ -7, 7 ≤ l ≤ -7	9 ≤ h ≤ -9, 10 ≤ k ≤ -10, 12 ≤ l ≤ -12	8 ≤ h ≤ -8, 9 ≤ k ≤ -9, 19 ≤ l ≤ -19

5. Cryogenic TEM screening

Milligram to sub-milligram quantities of dry powder were placed into a dram vial as received and manually ground with a glass pipette. A pure carbon 200 mesh Cu grid or lacey carbon Cu grid was placed inside of the vial and gently shaken together with the powder to “dry load” the grid. The grid was removed with Dumont straight self-closing tweezers and the tweezers were gently tapped against a lab bench while holding the grid to shake off excess powder. This sample was clipped into a Gatan 626 cryo holder at room temperature and inserted into a well-aligned Thermo Fisher Scientific Talos F200C transmission electron microscopy operating at an accelerating voltage of 200keV. After successful insertion, the cryo holder was cooled with liquid nitrogen until reaching a stable temperature of 80 K. After achieving stable temperature and low vacuum pressure, incident diffraction screening and movie collection were performed as described in Supporting Information, Section 2. Screening was halted after 3 hours, or if a preliminary solution with >90% of expected atoms was obtained. Results for samples collected in cryogenic temperatures are observed in Figure S4 and Table S3.

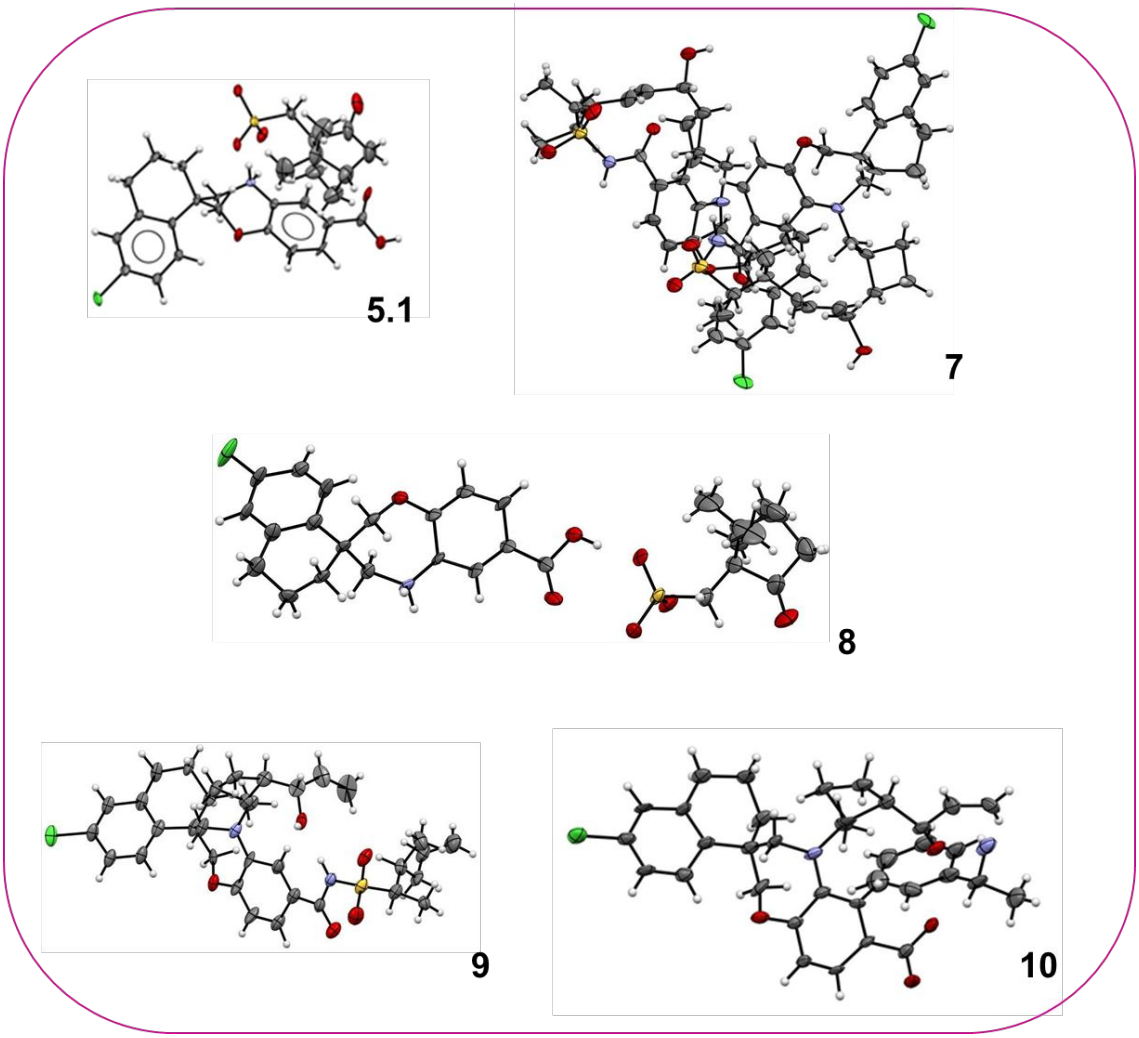

Figure S4. Contents of the asymmetric unit of compounds **5.1**, and **7**-**10** obtained at cryogenic temperature screening. Ellipsoids probability: 50 %

Table S3. Selected crystallographic data for compounds **5.1**, and **7**-**10** screened at cryogenic temperature.

Compound	**5.1**	**7**	**8**	**9**	**10**
Empirical formula	$C_{29}H_{34}NO_7SCl$	$C_{32}H_{39}N_2O_5SCl$	$C_{29}H_{34}NO_7SCl$	$C_{34}H_{43}N_2O_5SCl$	$C_{35}H_{36}N_2O_4Cl$
Formula weight	574.07	599.16	576.08	626.26	584.11
Data Collection					
Type of instrument	Talos F200C	Talos F200C	Talos F200C	Talos F200C	Talos F200C
Wavelength (Å)	0.0251	0.0251	0.0251	0.0251	0.0251
Data collection temperature (K)	96(4)	96(4)	96(4)	96(4)	96(4)
Unit cell dimensions	*a* = 10.4700(10) Å, *b* = 10.260(2) Å, *c* = 12.440(4) Å, *β* = 109.92 °	*a* = 11.3400(10) Å, *b* = 11.340(2) Å, *c* = 12.500(4) Å, *α* = 73.74 °, *β* = 69.36 °, *γ* = 71.13 °	*a* = 10.6900(10) Å, *b* = 10.220(2) Å, *c* = 12.680(4) Å, *β* = 111.22 °	*a* = 10.5200(10) Å, *b* = 15.050(2) Å, *c* = 17.020(4) Å	*a* = 7.9800(10) Å, *b* = 11.730(2) Å, *c* = 28.850(4) Å
Volume	1256.4(5)	1398.2(5)	1291.4(5)	2694.7(8)	2700.5(7)
Z, Z'	2, 1	2, 2	2, 1	4, 1	4, 1
Crystal system	Monoclinic	Triclinic	Monoclinic	Orthorhombic	Orthorhombic
Space group	$P2_1$	$P1$	$P2_1$	$P2_12_12_1$	$P2_12_12_1$
Density (calculated) (g/cm^3)	1.523	1.423	1.482	1.546	1.437
F(000)	99	243	99	105	103
Measured reflections	2474	6522	3824	2393	3263
Reflections with I > 2s(I)	1787	3782	2409	1774	2351
Resolution (Å)	1.00	0.90	0.85	1.00	0.85
Completeness (%)	92.60	82.50	85.20	83.10	68.60
Index ranges	10 ≤ h ≤ -10, 10 ≤ k ≤ -10, 12 ≤ l ≤ -12	12 ≤ h ≤ -12, 12 ≤ k ≤ -12, 13 ≤ l ≤ -13	12 ≤ h ≤ -12, 11 ≤ k ≤ -11, 14 ≤ l ≤ -14	10 ≤ h ≤ -10, 15 ≤ k ≤ -15, 15 ≤ l ≤ -14	9 ≤ h ≤ -9, 13 ≤ k ≤ -13, 25 ≤ l ≤ -25

6. Additional screening and recrystallization of samples

Crystallization of **11**, **13**, and **14** was performed by placing ~1 mg of powder as received into 6 x 50 mm borosilicate culture tubes purchased from VWR. Samples were dissolved in approximately 500 uL of solvent and allowed to slowly evaporate at room temperature. Higher boiling solvents were evaporated from open containers, while low boiling solvents required placing the culture tube inside an empty dram vial with a slightly loosened cap. If the initial solvent failed to produce a solid after fully evaporating based on visual inspection, the amorphous samples were re-dissolved in the same culture tube with a new solvent mixture. Evaporation occurred until precipitation was observed. Sample crystallization time spanned from overnight to 3 days. Samples **11** and **13** were obtained from slow evaporation from a 50/50 mixture of acetonitrile and water. The crystals were dried under reduced pressure. Sample **14** was crystallized from slow evaporation of diethyl ether. The crystals were placed onto a grid as dry powder. All crystals were screened at cryogenic temperatures as outlined in Supporting Information, section 3. Before typical screening, the prepared grid was plunged frozen in liquid nitrogen and transferred into the TEM while the holder was maintained at cryogenic temperatures. Sample **15** was generated from slow evaporation from H2O with a small amount of DMSO (10% v/v). The crystals were blotted with a kimwipe and dried under reduced pressure to remove excess solvent before diffraction experiments in cryogenic temperature. Sample **12** was screened in the same manner as described in Supporting Information, section 2 for ~4 additional hours at room temperature to locate monocrystalline domains in a largely polycrystalline sample.

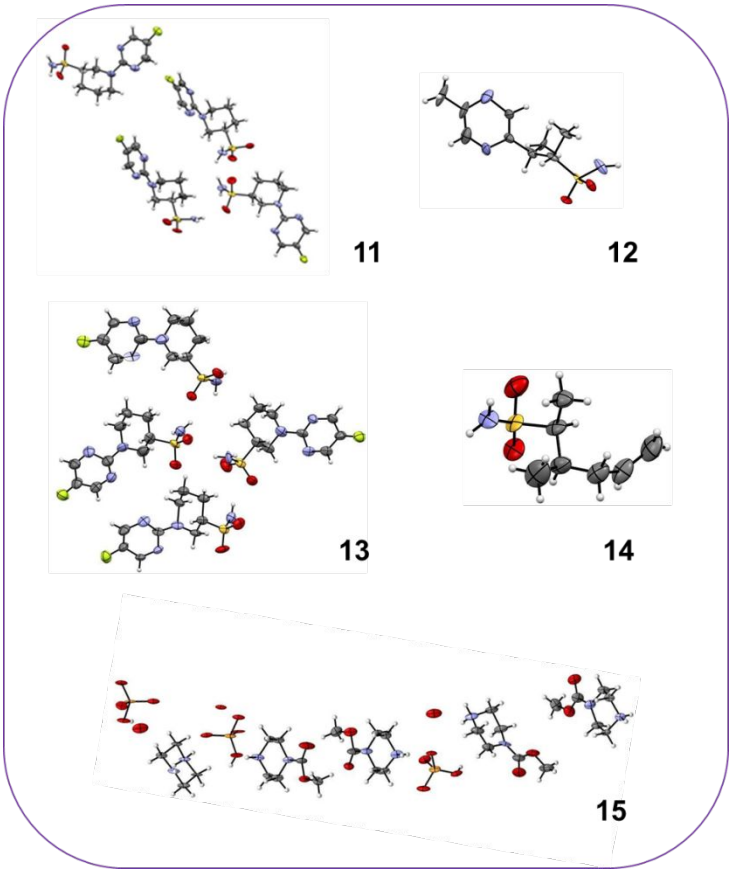

Figure S5. Contents of the asymmetric unit of compounds **11**-**15** obtained after additional screening and recrystallization trials. Ellipsoids probability: 50 %

Table S4. Selected crystallographic data for compounds **11**-**15** obtained after additional screening and recrystallization trials.

Compound	**11**	**12**	**13**	**14**	**15**
Empirical formula	$C_9H_{13}N_4O_2SF$	$C_9H_{15}N_3O_2S$	$C_9H_{13}N_4O_2SF$	$C_7H_{15}NO_2S$	$C_{28}H_{66}N_{10}O_{23}P_3$
Formula weight	260.29	229.3	260.29	177.26	1003.82
Data Collection					
Type of instrument	Talos F200C	Talos F200C	Talos F200C	Talos F200C	Talos F200C
Wavelength (Å)	0.0251	0.0251	0.0251	0.0251	0.0251
Data collection temperature (K)	96(4)	294(4)	96(4)	96(4)	96(4)
Unit cell dimensions	*a* = 22.990(2) Å, *b* = 37.240(4) Å, *c* = 4.6400(10) Å	*a* = 22.0000(10) Å, *b* = 6.410(2) Å, *c* = 7.060(4) Å, *β* = 91.18 °	*a* = 23.000(2) Å, *b* = 38.090(4) Å, *c* = 4.6000(10) Å	*a* = 7.4100(10) Å, *b* = 9.270(2) Å, *c* = 12.490(4) Å	*a* = 66.2000(10) Å, *b* = 6.220(2) Å, *c* = 9.940(4) Å, *β* = 92.14 °
Volume	3972.5(10)	995.4(4)	4029.9(10)	857.9(4)	4090(2)
Z, Z'	16, 4	4, 1	16, 4	4, 1	4
Crystal system	Orthorhombic	Monoclinic	Orthorhombic	Orthorhombic	Monoclinic
Space group	$P2_12_12$	$C2$	$P2_12_12$	$P2_12_12_1$	Cc
Density (calculated) (g/cm^3)	1.741	1.530	1.716	1.372	1.630
F(000)	43	49	170	29	169
Measured reflections	4964	1265	4939	1002	5976
Reflections with I > 2s(I)	3031	789	3181	461	3714
Resolution (Å)	0.90	0.90	0.90	0.90	0.85
Completeness (%)	83.10	86.50	82.60	80.30	84.6
Index ranges	25 ≤ h ≤ -25, 37 ≤ k ≤ -36, 5 ≤ l ≤ -5	24 ≤ h ≤ -24, 7 ≤ k ≤ -7, 7 ≤ l ≤ -7	25 ≤ h ≤ -25, 38 ≤ k ≤ -38, 5 ≤ l ≤ -5	8 ≤ h ≤ -8, 9 ≤ k ≤ -9, 12 ≤ l ≤ -12	70 ≤ h ≤ -71, 7 ≤ k ≤ -7, 11 ≤ l ≤ -11

7. Transmission electron microscope images of crystals

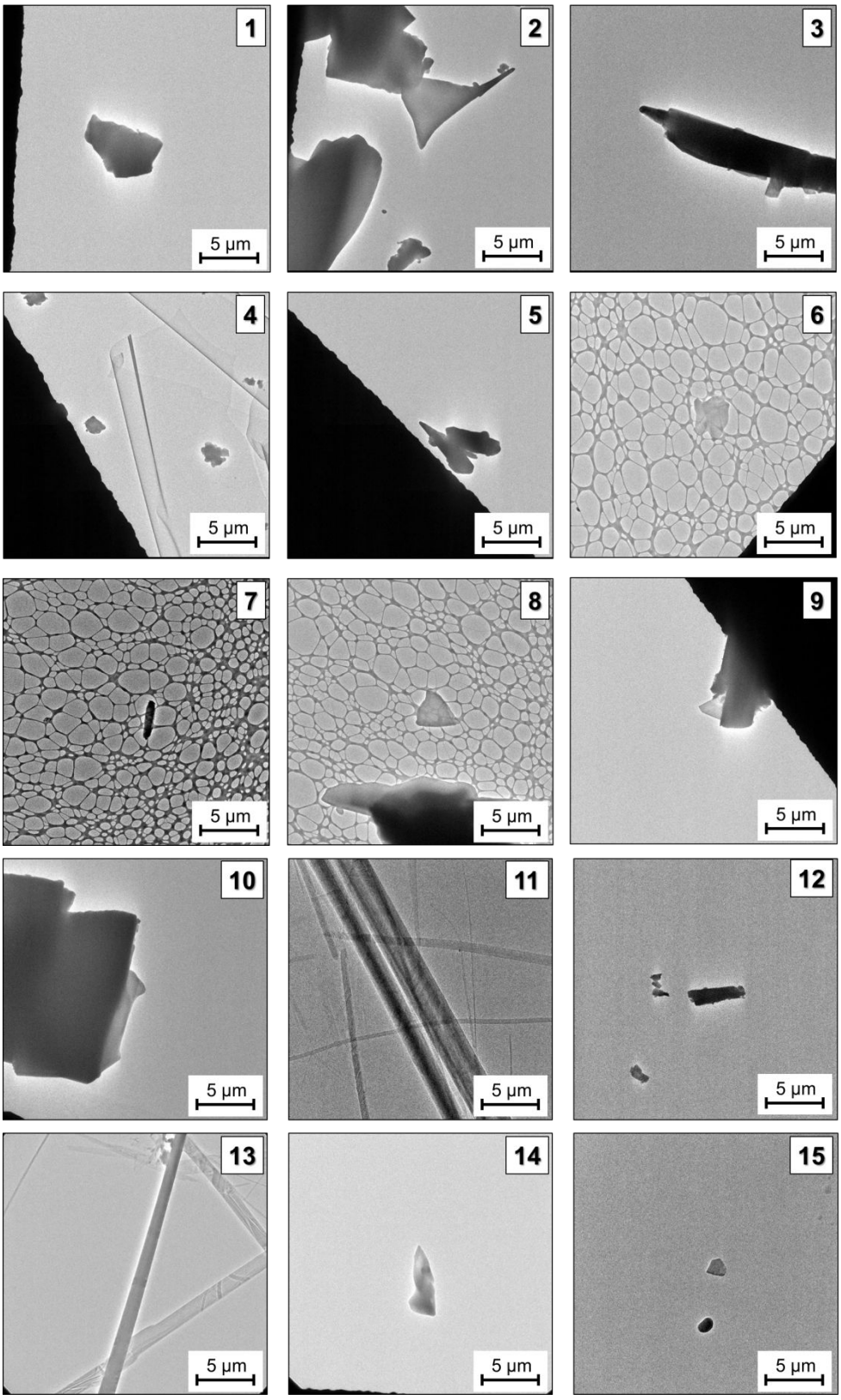

Figure S6. TEM image of crystals **1**-**15** at 2600x magnification.

8. Automated data processing procedure

Given the ability to collect multiple datasets in a matter of minutes, to further expedite structural analysis, we wanted the ability for a single user to simultaneously collect and process data. To facilitate this, our laboratory has developed a Python script that interacts with existing programs utilized for processing microED data to allow for automated conversion and indexing, inspired by similar automation developed for serial rotation electron diffraction [9].

Movie files are saved with sample name, detector distance, stage rotation speed, camera integration time, and rotation angle, allowing for automated importing of these values into the processing software, as follow:

samplename-mov1_960_0.3_3_cryo.ser

Where samplename-mov1 can be any name not including an underscore or special character, as this will become the name of the folder containing processed data, 960 is the detector distance used (in mm), 0.3 is the rotation speed of the stage (in °/s), 3 is the image integration time (in s), and cryo can be any additional notes about the sample and can include underscores.

On a computer running Ubuntu Windows Subsystem for Linux with properly installed XDS suite and the free ser2smv2 data conversion file [15], “python3 auto_indexing.py” is called to run Python3.8 in a folder containing an executable copy of ser2smv, the python scripts, and the .ser movie files to be processed. Merging and solutions obtained subsequent to autoprocessing were done by the user.

After executing the Python script, an open source movie conversion program is called to convert each SER movie to individual SMV frames (ser2smv) [15]. After conversion, the Python script writes a custom XDS.INP file with the appropriate settings based on our TEM settings and attempts to index and integrate frames using XDS [16]. The script is capable of detecting errors commonly encountered from our previous processing efforts and automatically corrects and re-subjects the data to XDS processing as needed until the dataset is either successfully integrated, or an upper limit is reached and the data is determined to be unindexable by the automated program. Furthermore, the script generates and executes the scaling program XSCALE and converts the data to SHELX format using XDSCONV [17].

Once one or more processed movies are obtained, a user can either directly solve the data by using the SHELX software suite, or quickly merge multiple pre-processed datasets using XSCALE before submitting to SHELX. After obtaining these preliminary solutions from SHELXT or SHELXD, the data was refined using SHELXL within ShelXle. The script is available for download in the supporting information section.

9. Data processing for the kinematical approach.

A Python script was created by our laboratory to convert and pre-process the diffraction movies collected. In the first step of the conversion, movies were converted into individual SMV frames by the open source movie conversion program ser2smv [15]. After conversion, the Python script writes a custom XDS.INP file based on our TEM settings and attempts to index and integrate frames using XDS software. The script is capable of detecting errors commonly encountered from our previous processing efforts and automatically corrects and re-subjects the data to XDS processing as needed until the dataset is either successfully integrated, or an upper limit is reached and the data is determined to be unindexable by the automated program. Furthermore, the script generates and executes the scaling program XSCALE and converts the HKL file using XDSCONV [15–17]. From the processed diffraction movies, the user can either directly solve the data using the SHELX software suite, or quickly merge multiple pre-processed datasets using XSCALE before submitting to SHELX. After obtaining these preliminary solutions from SHELXT or SHELXD, the data was refined using SHELXL within ShelXle [18–21].

10. Data Processing for the dynamical approach.

To process the diffraction images with Pets2.0 software [22], it was noted that images converted with ser2smv software were rotated counterclockwise (-90 °) and vertically flipped in comparison with the movies collected in the microscope. Thus, after converting the images from SMV to TIFF 16-bit format using an in house script, the TIFF images were further processed by rotating and flipping the images to the correct orientation.

All dynamical refinement experiments were performed in a single movie. Before processing the data with Pets software, all movies collected in the previous microED experiment were screened and diffraction datasets with the best statistics were chosen for dynamical refinement (typically movies with completeness higher than 70 %, resolution lower than 1.0 A and I/sigma higher than 2.0.

Electron diffraction data were imported to Pets2.0 software, with λ = 0.0251 Å, aperpixel = 0.00123 $Å^{-1}$, bin = 2, in the continuous rotation mode where rotation semi-angle was 0.45 °. The angle of the first frame (α) varied according to the diffraction movie collected, and the steps of rotation (α step) was fixed as 0.9 °. Data were processed with fixed GY = 26 and Ψ = 780 as all data was collected with the same Ceta-D detector. The beam stop was added manually for each sample and images were centered manually using the Friedel pairs option. The peak search was carried out with a reflection diameter varying between 3 and 10 pixels, and I/σ varying between 3 and 30. The rotation of the tilt axis around ω = 0 ° was performed and the peak analysis tool was used to check the quality of the reflections obtained. The initial unit cell was found and refined considering the refinement of the unit cell and distortions according to the correct symmetry. When necessary, the unit cell was manually transformed using the transformation matrix tool to match the results obtained with XDS.

Initial processing of the frames for integration was performed with the intensity determination method of sum counts, where the rocking curve and mosaicity values were initially set to 0.001. Once the camel plot was established, both parameters were optimized until a reliable fit between the curves was obtained. Frame geometry was optimized with uniform intensity considering the distortions and with polynomial smoothing correction of the angles with order 4. The frames were again processed for integration with the fit profile option and integration was finalized with the intensity estimation "integrate profile", choosing the correct Laue class, refining the error model, and with automatic virtual frame parameters. This process generates two files: *XX*.cif_pets for kinematical solution and refinement and *XX*_dyn.cif_pets file for dynamical refinement of the crystal structures.

11. Kinematical and Dynamical Refinement with Jana2020.

For the kinematical refinement of the crystal structure using Jana2020 software [23], the *XX*.cif_pets file was imported and the crystal structure was solved with Shelxt within Jana2020 suite. When solution of the kinematical structure was not possible, the CIF or INS files were imported in the software and refined with isotropic atoms against the *XX*.cif_pets file. Hydrogens were positioned using fixed restraints with typical neutron distances and when necessary interatomic distances and angles were fixed. Samples **8** and **11** were refined with fixed coordinates. All kinematic solutions were refined with 10 cycles of refinement, enabling atoms with too large isotropic ADPs and on F^2.

For dynamical refinement, the *XX*_dyn.cif_pets reflection file was imported in the software for refinement against the structural model. Thickness plots were obtained by optimizing the thickness with RSg(max) was fixed to 0.66 while g(max) was set according to the sample, and general EDThick parameter was obtained based on thickness plots. Dynamical refinement was carried out with 10 cycles of refinement, enabling atoms with too large isotropic ADPs and on F. Once the refinement of the structure was concluded, the enantiomorph was inverted and the same refinement procedure was performed. Both enantiomeric pairs refined with dynamical refinement had their chirality assigned by the geometry tool within Platon software [24]. The correct enantiomer is assigned by the crystal structures with lower values of R(obs), wR(obs), R(all), and wR(all).

12. Dynamical refinement results

Table S5. Statistics of the movies selected for dynamical refinement processed with XDS and Pets2.0.

Sample	Movie #	Rotation of sample	XDS					Pets2.0				
			Resolution (Å)	Completeness (%)	R-factor (obs) (%)	Mean I/σ	CC (1/2)	Resolution (Å)	Completeness (%)	I/σ	Rint (obs) (%)	Rint(all) (%)
1	4	p45n50	0.90	71.5	9.9	4.79	98.1	0.83	79	3.77	15.06	15.71
2	2	n60p60	0.90	82.9	16.5	5.97	99.2	0.89	87	2.97	18.43	19.16
3	1	p60n60	0.90	65.3	14.8	5.12	98.5	0.91	69	3.75	20.74	21.23
4	2	n60p60	1.00	88.7	38.9	4.19	96.5	1	91	3.27	19.21	20.19
5	9	n65p60	0.90	79.9	14.1	4.69	98.4	1	92	3.62	17.17	17.53
6	1	n50p50	0.85	98.3	15.6	5.06	98.6	0.86	100	2.91	20.24	21.86
7	6	n60p60	0.90	49.5	9.1	5.72	97.8	0.88	56	6.71	11.14	11.37
8	4	n60p60	1.10	78.3	14.1	4.72	97.2	0.95	82	3.08	21.95	23.78
9	8	p60n45	0.90	90.7	22.1	4.40	97.8	0.83	93	2.69	22.86	24.31
10	12	n60p50	1.10	75.4	28.3	5.06	97.6	1	77	2.55	25.89	27.25
11	25	p65n20	0.90	81.2	16.9	5.00	98.7	1	83	2.39	21.98	25.73
12	7	n60p60	0.90	76.8	12.6	5.73	99.1	0.91	79	3.86	15.96	16.42
13	16	p30n50	0.90	77.4	13.1	5.48	99.4	0.91	80	3.33	18.59	20.38
14	5	p40n30	0.90	72.5	13.4	4.31	99.2	0.83	76	2.91	18.22	19.67

Table S6. Kinematic and dynamical refinements statistics. Dynamical refinement (dyn) for enant 1 (structure as solved) and enant 2 (inverted enantiomer). Samples **8** and **11** were refined with fixed atomic coordinates. All samples were refined with isotropic atoms.

Sample	Kinematic solution	Refinement with Jana2020							
		Type of refinement	R-factors	GOF_{obs}	GOF_{all}	R_{obs} (%)	wR_{obs} (%)	R_{all} (%)	wR_{all} (%)
1	microED CIF imported	Kinematical	[6707=4211+2496/297]	2.26	1.99	25.47	51.71	26.82	54.65
		Dyn – enant 1	[7466=2807+4659/342]	4.16	2.61	12.59	11.60	18.73	12.21
		Dyn – enant 2	[7466=2807+4659/342]	5.37	3.33	15.55	14.95	22.18	15.59
2	Shelxt on Jana	Kinematical	[1448=1091+357/65]	2.38	2.19	23.22	47.98	24.47	49.63
		Dyn – enant 1	[5592=1537+4055/130]	5.00	2.69	15.10	15.16	23.14	15.70
		Dyn – enant 2	[5592=1537+4055/130]	4.28	2.33	13.07	12.97	21.50	13.59
3	microED CIF imported	Kinematical	[4315=2649+1666/297-2]	2.47	2.06	22.88	45.67	24.64	47.86
		Dyn – enant 1	[8214=3187+5027/362]	4.75	3.01	14.40	14.10	20.76	14.73
		Dyn – enant 2	[8214=3187+5027/362]	3.95	2.54	12.47	11.74	18.67	12.41

Sample	Kinematic solution	Refinement with Jana2020							
		Type of refinement	R-factors	GOF_{obs}	GOF_{all}	R_{obs} (%)	wR_{obs} (%)	R_{all} (%)	wR_{all} (%)
4	microED CIF imported	Kinematical	[1468=620+848/65]	2.94	2.34	23.28	28.06	35.32	32.46
		Dyn – enant 1	[3924=561+3363/130]	2.63	1.11	10.44	9.07	24.41	10.51
		Dyn – enant 2	[3924=561+3363/130]	2.84	1.21	11.13	9.82	26.12	11.45
5	microED CIF imported	Kinematical	[2457=1896+561/157]	2.15	2.05	21.15	46.29	22.74	49.14
		Dyn – enant 1	[3536=1339+2197/225]	2.77	1.82	10.50	9.30	17.19	10.26
		Dyn – enant 2	[3536=1339+2197/225]	3.63	2.33	13.36	12.20	20.05	13.10
6	Shelxt on Jana	Kinematical	[1618=1206+412/61]	2.69	2.47	32.20	59.06	32.71	60.85
		Dyn – enant 1	[3768=1651+2117/120]	6.27	4.20	16.25	16.50	21.58	16.85
		Dyn – enant 2	[3768=1651+2117/120]	5.52	3.71	14.47	14.53	19.61	14.87
7	microED CIF imported	Kinematical	[4830=3681+1149/329]	3.83	3.48	22.39	29.01	25.35	30.13
		Dyn – enant 1	[4637=2207+2430/382]	4.16	2.90	13.00	12.40	17.88	13.01
		Dyn – enant 2	[4637=2207+2430/382]	4.89	3.38	15.12	14.57	20.48	15.2
8	microED CIF imported	Kinematical	[2203=1182+1021/40]	2.52	2.16	21.57	28.01	26.01	30.53
		Dyn – enant 1	[3053=752+2301/104]	5.02	2.58	15.15	14.88	24.61	15.61
		Dyn – enant 2	[3053=752+2301/104]	5.78	2.95	16.24	17.13	25.72	17.81
9	microED CIF imported	Kinematical	[4749=2906+1843/173]	2.05	1.89	21.05	45.24	24.62	50.55
		Dyn – enant 1	[11022=3085+7937/229]	3.11	1.73	11.01	10.34	18.06	10.99
		Dyn – enant 2	[11022=3085+7937/229]	4.81	2.61	15.90	15.97	23.11	16.61
10	microED CIF imported	Kinematical	[2273=1598+675/169]	1.96	1.80	19.67	41.85	22.32	44.34
		Dyn – enant 1	[6576=985+5591/228]	2.06	1.03	9.85	8.92	23.06	12.09
		Dyn – enant 2	[6576=985+5591/228]	2.52	1.18	11.79	10.94	24.48	13.80
11	microED CIF imported	Kinematical	[3702=1605+2097/69]	2.09	1.71	17.65	25.85	25.60	28.66
		Dyn – enant 1	[7659=1216+6443/115]	3.80	1.63	13.83	12.76	39.75	13.91
		Dyn – enant 2	[7659=1216+6443/115]	4.57	1.92	15.88	15.63	32.22	16.41
12	Shelxt on Jana	Kinematical	[1145=840+305/61]	2.33	2.13	23.27	46.56	24.55	48.45
		Dyn – enant 1	[1785=617+1168/126]	3.34	2.04	11.84	10.79	18.19	11.51
		Dyn – enant 2	[1785=617+1168/126]	2.56	1.59	9.30	8.29	15.51	8.95
13	microED CIF imported	Kinematical	[4814=2305+2509/273]	2.46	1.95	16.55	22.14	26.81	24.96
		Dyn – enant 1	[9950=1468+8482/318]	3.28	1.30	10.38	8.77	27.51	9.84
		Dyn – enant 2	[9950=1468+8482/318]	4.48	1.76	14.08	12.00	34.31	13.31
14	microED CIF imported	Kinematical	[1156=620+536/45]	3.08	2.69	28.21	36.50	33.71	40.14
		Dyn – enant 1	[2035=711+1324/82]	7.12	4.25	17.99	19.25	27.50	19.78
		Dyn – enant 2	[2035=711+1324/82]	6.30	3.78	16.84	17.03	25.63	17.57

Table S7. Statistical results using enantprob software for enantiomeric pairs analyzed with dynamical refinement. Enant represents the order the files were input in the enantprob software, where enant1 is the structure as solved and enant2 is the inverted structure.

Sample	Enant	Total	better for 1	better for 2	prob(wrong)	sigma level	prob(1)	Rval1	Rval2	Rval2/1
1	1	5376	3132	2244	2091	12.111	1.000000	18.693	22.143	1.185
	2	7466	4177	8289	0	10.277	1.000000			
2	2	3533	1893	1640	2058	4.256	0.999990	21.313	22.937	1.076
	1	5591	2922	2669	0	3.384	0.999642			
3	2	5839	3200	2639	2374	7.342	1.000000	18.646	20.727	1.112
	1	8213	4387	3826	0	6.190	1.000000			
4	1	2296	1249	1047	1628	4.216	0.999988	24.118	25.815	1.070
	2	3924	2063	1861	0	3.225	0.999369			
5	1	2438	1409	1029	1099	7.696	1.000000	17.159	20.005	1.166
	2	3536	1958	1578	0	6.390	1.000000			
6	2	2610	1446	1164	1159	5.520	1.000000	19.568	21.536	1.101
	1	3768	2025	1743	0	4.594	0.999998			
7	1	3575	2022	1553	1062	7.844	1.000000	17.851	20.452	1.146
	2	4637	2553	2084	0	6.887	1.000000			
8	1	1855	931	924	1198	0.163	0.564555	24.442	25.544	1.045
	2	3053	1530	1523	0	0.127	0.550406			
9	1	7388	4523	2865	3635	19.290	1.000000	17.990	23.017	1.279
	2	11022	6340	4682	0	15.793	1.000000			
10	1	4000	2146	1854	2576	4.617	0.999998	22.950	24.367	1.062
	2	6576	3434	3142	0	3.601	0.999841			
11	1	4747	2614	2133	2912	6.981	1.000000	28.909	31.311	1.083
	2	7659	4070	3589	0	5.496	1.000000			
12	2	1195	675	520	591	4.484	0.999996	15.459	18.139	1.173
	1	1785	970	815	0	3.669	0.999878			
13	1	6414	3968	2446	3537	19.004	1.000000	26.555	33.119	1.247
	2	9950	5736	4214	0	15.258	1.000000			
14	2	1481	790	691	555	2.573	0.994952	25.503	27.365	1.073
	1	2035	1067	968	0	2.195	0.985903			

13. Single crystal X-ray diffraction

All crystals were measured using a Bruker Venture D8 diffractometer, at 100 K, with Mo Kα (λ = 0.7107 Å) or Cu Kα (λ = 1.5418 Å) radiation. The reflection images (.srmf file) were imported into the software CrysAlis Pro and processed with the smart peak search and background. SHELXS or SHELXT were used for the structure solution and refinement was performed with SHELXL-2014 [17-20], all implemented within the WinGX suite [25]. All atoms, except hydrogen, had atomic coordinates and anisotropic thermal parameters refined to convergence using full-matrix least-square methods on F^2. Hydrogen atoms bound to carbon atoms were placed in geometric positions and refined with riding modes. Hydrogen atoms bound to nitrogen atoms were found by difference syntheses and refined with isotropic displacement parameters. The correct enantiomer was assigned by the values of the Flack parameter and using Platon software [24].

Table S8. Selected crystallographic data for compounds **1**, **3**, **6**, and **11** obtained by single crystal X-ray diffraction (XRD).

	1_XRD	**3_XRD**	**6_XRD**	**14_XRD**
Empirical formula	$C_{25}H_{29}N_7O_4S$	$C_{25}H_{29}N_7O_4S$	$C_9H_{15}N_3O_2S$	$C_7H_{15}NO_2S$
Formula weight	523.61	523.61	229.3	177.26
Temperature (K)	100(2)	100(2)	100(2)	100.00(10)
Crystal system	monoclinic	monoclinic	orthorhombic	orthorhombic
Space group	$P2_1$	$P2_1$	$P2_12_12_1$	$P2_12_12_1$
Unit cell dimensions	*a* = 9.62380(10) Å, *b* = 21.3832(2) Å, *c* = 12.97770(10) Å, *β* = 107.7100(10) °	*a* = 9.6182(2) Å, *b* = 21.3742(4) Å, *c* = 12.9746(3) Å, *β* = 107.681(2) °	*a* = 7.52000(10) Å, *b* = 8.4522(2) Å, *c* = 17.0377(3) Å	*a* = 7.68240(10) Å, *b* = 9.8732(2) Å, *c* = 12.6237(3) Å
Volume (Å^3)	2544.08(4)	2541.34(10)	1082.93(4)	957.51(3)
Z	2	2	4	4
ρ_{calc} (g/cm^3)	1.367	1.369	1.406	1.230
μ/mm^{-1}	1.519	1.521	0.284	2.669
F(000)	1104	1104	488	384
Radiation	CuKα (λ = 1.54184)	CuKα (λ = 1.54184)	MoKα (λ = 0.71073)	CuKα (λ = 1.54184)
2Θ range for data collection (°)	7.15 to 158.544	7.15 to 158.716	4.782 to 52.742	11.378 to 158.054
Index ranges	-12 ≤ h ≤ 11, -27 ≤ k ≤ 26, -16 ≤ l ≤ 16	-12 ≤ h ≤ 12, -25 ≤ k ≤ 27, -16 ≤ l ≤ 16	-9 ≤ h ≤ 9, -10 ≤ k ≤ 10, -21 ≤ l ≤ 21	-9 ≤ h ≤ 9, -12 ≤ k ≤ 12, -16 ≤ l ≤ 16
Reflections collected	71284	53858	14483	12054
Independent reflections	10702 [R_{int} = 0.0638, R_{sigma} = 0.0315]	10584 [R_{int} = 0.1225, R_{sigma} = 0.0805]	2217 [R_{int} = 0.0838, R_{sigma} = 0.0365]	2028 [R_{int} = 0.0510, R_{sigma} = 0.0338]
Data/restraints/parameters	10702/1/680	10584/1/679	2217/0/145	2028/0/120
Goodness-of-fit on F^2	1.079	1.031	1.084	1.040
Final R indexes [I>=2σ (I)]	R_1 = 0.0382, wR_2 = 0.1049	R_1 = 0.0494, wR_2 = 0.1194	R_1 = 0.0345, wR_2 = 0.0898	R_1 = 0.0292, wR_2 = 0.0735
Final R indexes [all data]	R_1 = 0.0387, wR_2 = 0.1054	R_1 = 0.0639, wR_2 = 0.1338	R_1 = 0.0350, wR_2 = 0.0901	R_1 = 0.0333, wR_2 = 0.0759
Largest diff. peak/hole (e Å^{-3})	0.31/-0.33	0.29/-0.31	0.45/-0.37	0.20/-0.24
Flack parameter	0.006(11)	-0.010(16)	0.05(7)	-0.005(12)

14. References

(1) PCT Int. Appl. 2016, WO 2016187308 A1 20161124.
(2) PCT Int. Appl. 2018, WO 2018097945 A1 20180531.
(3) PCT/US2015/047472, WO 2016033486 A1.
(4) PCT Int. Appl. 2018, WO 2018093576 A1 20180524.
(5) PCT Int. Appl. 2018, WO 2018093577 A1 20180524.
(6) PCT Int. Appl. 2018, WO 2018093579 A1 20180524.
(7) PCT Int. Appl. 2018, WO 2018097944 A1 20180531.
(8) PCT Int. Appl. 2018, WO 2018097945 A1 20180531.
(9) Hattne, J., et al. Acta Cryst. 2015, 71, 353–360.
(10) PCT Int. Appl. 2019, WO 2019006231 A1 20190103.
(11) PCT Int. Appl. 2016, WO 2016141035 A1.
(12) J. Org. Chem. 2014, 79, 3684–3687.
(13) J. Med. Chem. 2014, 57, 9796–9810.
(14) J. Med. Chem. 2018, 61, 453–461.
(15) Program ser2smv obtained from https://cryoem.ucla.edu/downloads/snapshots
(16) Acta Cryst. 2010, D66, 125–132.
(17) Acta Cryst. 2010, D66, 133–144.
(18) Acta Cryst. 2008, A64, 112–122.
(19) Acta Cryst. 2015 A71, 3–8.
(20) Acta Cryst. 2015, C71, 3–8.
(21) J. Appl. Cryst. 2011, 44, 1281–1284.
(22) Acta Crystallogr. Sect. B Struct. Sci. Cryst. Eng. Mater. 2019, 75 (4), 512–522.
(23) Cryst. Mater. 2023, 238 (7-8), 271-282.
(24) Acta Cryst. 2009, D65, 148-155.
(25) J. Appl. Cryst. 1999, 32, 837-838.